

Article

Implementation of a Prediction Model in a Smart System for Enhancing Comfort in Dwellings

Snezhinka Zaharieva ¹, Ivan Georgiev ^{2,3}, Slavi Georgiev ^{2,3,*}, Jordan Stoev ¹ and Adriana Borodzhieva ⁴

- ¹ Department of Electronics, Faculty of Engineering, Electronics and Automation, University of Ruse, 8 Studentska Str., 7004 Ruse, Bulgaria; szaharieva@uni-ruse.bg (S.Z.); istoev@uni-ruse.bg (I.S.)
- ² Department of Informational Modeling, Institute of Mathematics and Informatics, Bulgarian Academy of Sciences, 8 Acad. Georgi Bonchev Str., 1113 Sofia, Bulgaria; irgeorgiev@math.bas.bg or irgeorgiev@uni-ruse.bg
- ³ Department of Applied Mathematics and Statistics, Faculty of Natural Sciences and Education, University of Ruse, 7004 Ruse, Bulgaria
- ⁴ Department of Telecommunications, Faculty of Engineering, Electronics and Automation, University of Ruse, 8 Studentska Str., 7004 Ruse, Bulgaria; aborodzhieva@uni-ruse.bg
- * Correspondence: sggeorgiev@uni-ruse.bg or sggeorgiev@math.bas.bg; Tel.: +359-82-888-623

Abstract: This article introduces a novel approach to ensuring optimal comfort in residential environments, using a smart system powered by predictive modeling. At its core lies a complex algorithm, presented alongside a detailed block diagram, guiding the system's operations, which are tailored for residential comfort. The primary focus is on the time series analysis of forecasting relative humidity—a critical parameter influencing comfort in living spaces. Among the various prediction models analyzed, a model based on the Fourier equation emerged as the most efficient, accounting for approximately 81% of variances in data. Upon validation, the model showcases an impressive relative error of just $\pm 0.1\%$. The research underscores the potential of leveraging advanced forecasting in optimizing devices like dehumidifiers or air humidifiers, ensuring the desired comfort while minimizing energy consumption. This innovative integration paves the way for a smarter, more sustainable residential living experience.

Keywords: forecasting; time series analysis; relative humidity; temperature; microclimatic parameters; living comfort; expenditure reduction; savings; IoT



Citation: Zaharieva, S.; Georgiev, I.; Georgiev, S.; Stoev, J.; Borodzhieva, A. Implementation of a Prediction Model in a Smart System for Enhancing Comfort in Dwellings. *Electronics* **2023**, *12*, 4899. <https://doi.org/10.3390/electronics12244899>

Academic Editors: Amedeo Andreotti and Bianca Caiazzo

Received: 23 October 2023
Revised: 30 November 2023
Accepted: 2 December 2023
Published: 5 December 2023



Copyright: © 2023 by the authors. Licensee MDPI, Basel, Switzerland. This article is an open access article distributed under the terms and conditions of the Creative Commons Attribution (CC BY) license (<https://creativecommons.org/licenses/by/4.0/>).

1. Introduction

It is important to note that, despite concerted efforts to establish a conducive microclimate within indoor environments, there has been a notable uptick in complaints regarding discomfort and health issues from the inhabitants of these spaces over recent years [1–4]. This makes the assessment of indoor air quality of paramount importance.

Thermal comfort exerts a direct influence on both the actual and perceived microclimatic conditions within an interior environment. This comfort level is a result of the interplay between factors such as temperature, relative humidity, air circulation, the metabolic rate of the inhabitants, and the thermal insulation properties of their attire [5–8].

The level of relative humidity in the air has a direct bearing on thermal comfort, which, in turn, impacts the health and well-being of the occupants of a given space [9,10]. It is crucial to maintain the relative humidity level in inhabited spaces at between 30 and 70% as this enables the inhabitants to feel comfortable [11–13].

In the era of Industry 4.0, electronic systems, remote control, and management modules are becoming the go-to technical solutions for both domestic and industrial applications. Industry 4.0 is intrinsically linked with the Internet of Things (IoT), integrating technology with manufacturing techniques, enabling systems to exchange, analyze, and utilize information for intelligent decision-making [14].

The future trajectory of IoT technology lies in predictive models. These models, anchored on various statistical and analytical techniques, aim to optimize the utilization of the developed IoT devices and systems. This, undoubtedly, will culminate in more intelligent actions [15,16].

The integration of predictive models into IoT devices and systems could very well become the groundbreaking technology that dominates future decades. Through this integration, the vast volume of data generated by the IoT devices/systems will facilitate Internet-connected objects to become increasingly smarter and more sophisticated.

In recent years, neural networks and artificial intelligence have become increasingly preferred approaches for the predictive modeling of various processes. The potential of neural networks and artificial intelligence cannot be denied, but the decision to use a classical time series model in the current study was made after careful consideration of the factors outlined below [17–19]:

- Classical time series models often provide greater interpretability compared to complex neural networks. In applications where understanding the relationships between variables is crucial, the transparency of a time series model can be advantageous. This is particularly relevant in our study, where the goal is to predict relative humidity to ensure comfortable and healthy conditions in a dwelling.
- The nature of the measured data from the developed smart system may not fully leverage the strengths of neural networks. If the dataset is relatively small or lacks the complexity that neural networks handle well, a simpler time series model can offer comparable results with a lower risk of overfitting.
- Classical time series models often require fewer computational resources and less training time compared to neural networks. In scenarios where computational efficiency is a priority, especially in real-time applications, a time series model can be more practical.
- Time series modeling has a well-established history in forecasting applications. The reliability and good results obtained with classical time series methods in various fields make them a suitable choice, especially when the goal is to achieve a balance between accuracy and simplicity.

It is known that the indoor relative humidity level in the air has a direct impact on the thermal comfort of the dwelling's residents, which in turn affects their health and well-being. Aiming for the latter, a smart system has been developed to optimize, control, and manage environmental factors using real-time data on microclimatic parameters.

The aim of this paper is to present an implemented time series predictive model, the task of which is to make a forecast in the near future (30 min) of the relative humidity in a room. Based on the obtained forecast, a control module of a humidifier or a dehumidifier is preventively triggered to provide a comfortable and healthy environment for the room's occupants.

This paper is organized as follows. In Section 2, the algorithm for the work of the smart system is presented in detail, and its structural scheme is thoroughly explained. In Section 3, the forecasting models are theoretically presented and the obtained results for the winter period are described. Then, the results are profoundly discussed. The paper concludes in Section 4 with the important implications of the results and possible future work directions are outlined.

2. Algorithm for the Work and Structural Scheme of a Smart System Enhancing Comfort in Dwellings

2.1. Algorithm for the Work of the Smart System Enhancing Comfort in Dwellings

The algorithm for work is shown in Figure 1. The cornerstone of the smart system is a communication node, referred to as Block 1, which facilitates connectivity among all the multifunctional sensor modules embodied in Blocks 2–4. Moreover, it links with an MQTT broker [20–23], allowing data interchange with the mobile application designed for control and monitoring (Block 5). The system also establishes a connection with a GPS receiver

to obtain an accurate astronomical time [24]. This communication node further ensures connectivity to a cloud server where microclimatic measurement data and the results from algorithmic energy flow models [25] are stored. The communication node encompasses a WiFi router, the primary system ensuring comfortable indoor conditions, a GPS receiver that provides precise timekeeping, and a personal computer to configure and visualize the specific parameters of the indoor comfort management system [26].

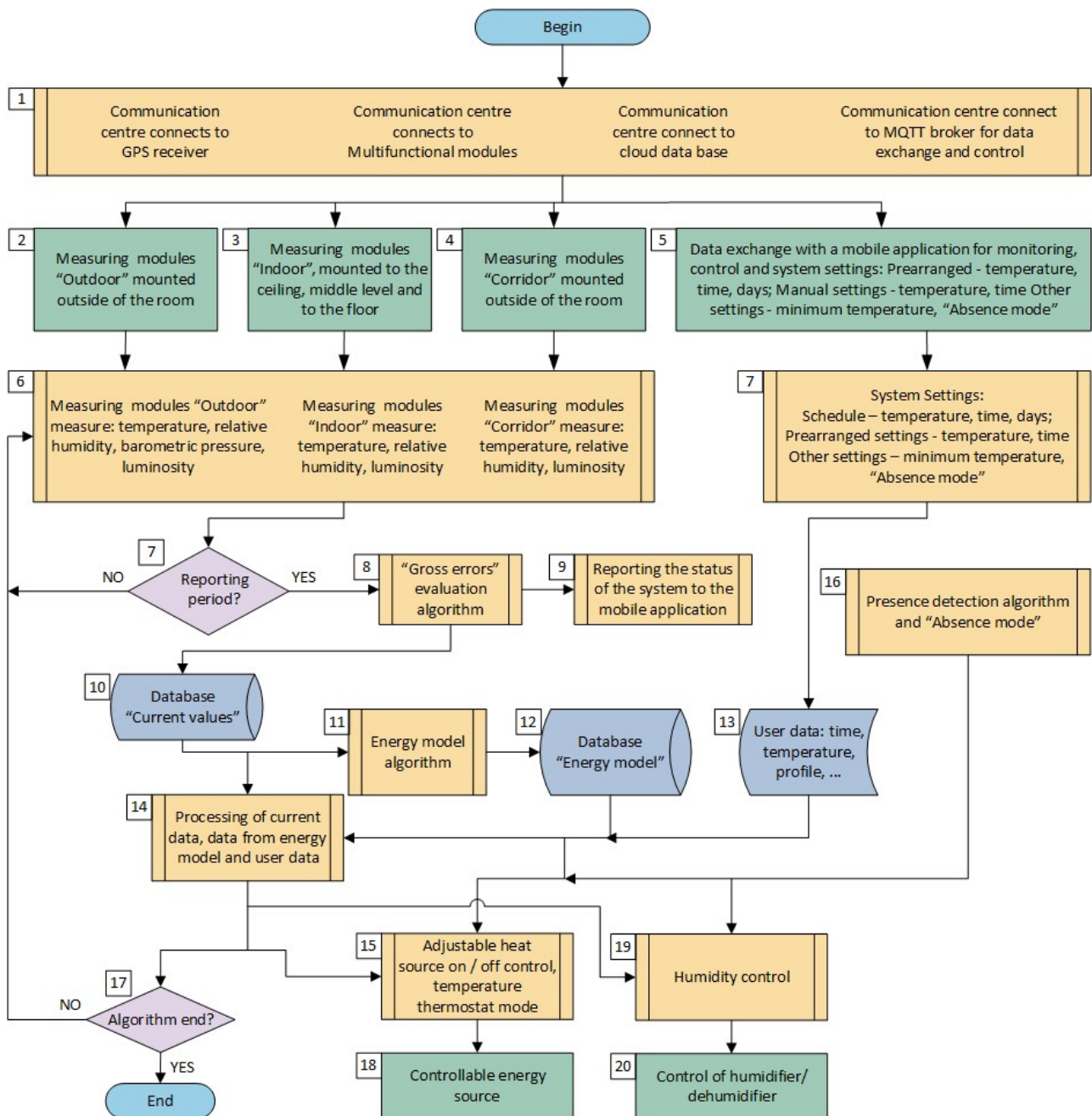


Figure 1. Algorithm for the operation of the smart system enhancing comfort in dwellings.

The DHCP server [27] within the WiFi router allocates IP addresses to all linked devices, having predefined the IP addresses for the multifunctional sensor modules and the system. This step is imperative as the system gathers measurement data by making real-time queries to each sensor.

The multifunctional sensor modules in Blocks 2–4 stand as the second most critical components of the smart system. Their primary responsibility is to gauge, with high

precision, the essential microclimatic indicators of the ambient environment, both inside the designated dwelling and outside it, within the building's corridor.

Block 5 manages communication with the mobile application and configures specific parameters within the system:

- Prearranged settings—indoor temperature, relative humidity, switch-on and switch-off times, and a weekly schedule.
- Manual configurations—indoor temperature, the target relative humidity, and the intended time to achieve them.
- Universal system configurations—IP address of MQTT broker, port of MQTT broker, and registered smartphones.
- Additional settings—the dwelling's minimum temperature and relative humidity, along with an "Absence mode".

The configurations are saved as a file in Block 7 and play a crucial role in both the analysis and the comprehensive functioning of the system. In the event of a power outage, these data points are utilized to reinstate normal operation.

In Block 6, using the measuring modules, continuous parameter measurements take place, periodically recording the acquired values. The duration of the reading cycle is determined in Block 7.

After the conclusion of the predetermined reporting period, the acquired data undergoes the statistical operation [28–30] in Block 8. This process ensures the derivation of precise measurement data from each specific point. The data, purged of any gross errors, is subsequently stored in Block 10 on a cloud server. In Block 9 of the algorithm, the system communicates its status to the mobile application, providing information on current temperatures, the relative humidity, and the condition of the sensors. This includes details on which temperature and humidity sensors are supplying valid data and which ones have been deactivated after statistical processing to eliminate gross errors.

The temperature data, after the removal of gross errors, serves as the input for Block 11 and Block 13, and the outcome of the operation in Block 11 is stored in Block 12 [31].

Data from Block 13 and other system settings reflecting the specific requirements of the dwelling's occupants for ensuring the necessary thermal comfort and reducing heating expenses are fed into Block 14. In various ways, the user determines this data, which is also stored on the cloud server. This lays the groundwork for the introduction of a predictive model that will autonomously learn from user data patterns and adapt the energy consumption within the dwelling without requiring any intervention from the resident.

Following the processes in Blocks 13 and 14, Block 15 identifies the times for activating and deactivating the "Adjustable heat source" in Block 18. Block 19 of the algorithm establishes humidity maintenance parameters according to predefined criteria. Once the range for humidity maintenance is specified, it provides the input for the humidity control system overseen by Block 20.

Decisions are made based on the input temperatures from the energy model, the time needed to achieve the desired temperature, the time to deactivate the heat source, or from Block 16, which detects the "Absence mode". The input data for Block 15 are:

- User data—the desired temperature and the time needed to achieve it, along with the time period for maintaining the temperature;
- Calculated temperature from the energy model, the overall energy heat exchange, and the measured temperature from the thermosensors;
- Presence of the user;
- "Absence mode";
- System time.

Traditional methods for identifying presence often employ sensors or infrared cameras [32–36]. Modern algorithms leverage neural networks and artificial intelligence to deduce the presence of an object within a designated space [37–39]. The intelligent system

developed utilizes smartphone detection, requiring prior registration of the device in the system. In Figure 1, Block 16 of the algorithm operates as a subroutine, checking the local network for the registered smartphone’s presence through its MAC address, utilizing the system utility PING. If there’s a smartphone with the matching MAC address, it will respond, thereby indicating presence. If there is no presence detected for more than 48 h, the system automatically switches to “Absence mode” mode and in Block 15, a mode is activated to maintain a minimum set temperature.

Humidity control in the algorithm from Figure 1 is executed by Block 19. Input data for Block 19 are:

- Relative humidity and temperature as measured by sensors;
- Presence of a user;
- “Absence mode”;
- System time.

Block 6 in the algorithm of Figure 1 remains active, and the succeeding blocks execute their tasks until the user initiates the activation of Block 17, “End of Work?” This action leads to the final “End” block.

Once the adjustable heat source is turned off, the smart system proceeds to a new cycle for determining energy flow, as well as one for determining the approximate moment for activating the heat source, dehumidifier, and humidifier.

2.2. Structural Scheme of a Smart System Enhancing Comfort in Dwellings

Figure 2 shows the logical structural diagram of the smart system, which has been designed to ensure comfortable conditions in a dwelling. In total, eight pairs of measuring modules are used to measure the microclimatic parameters, both inside and outside the dwelling. An adjustable heat source is implemented to achieve the desired temperature in the dwelling, and there is also a module that achieves humidity control by managing a dehumidifier and humidifier.

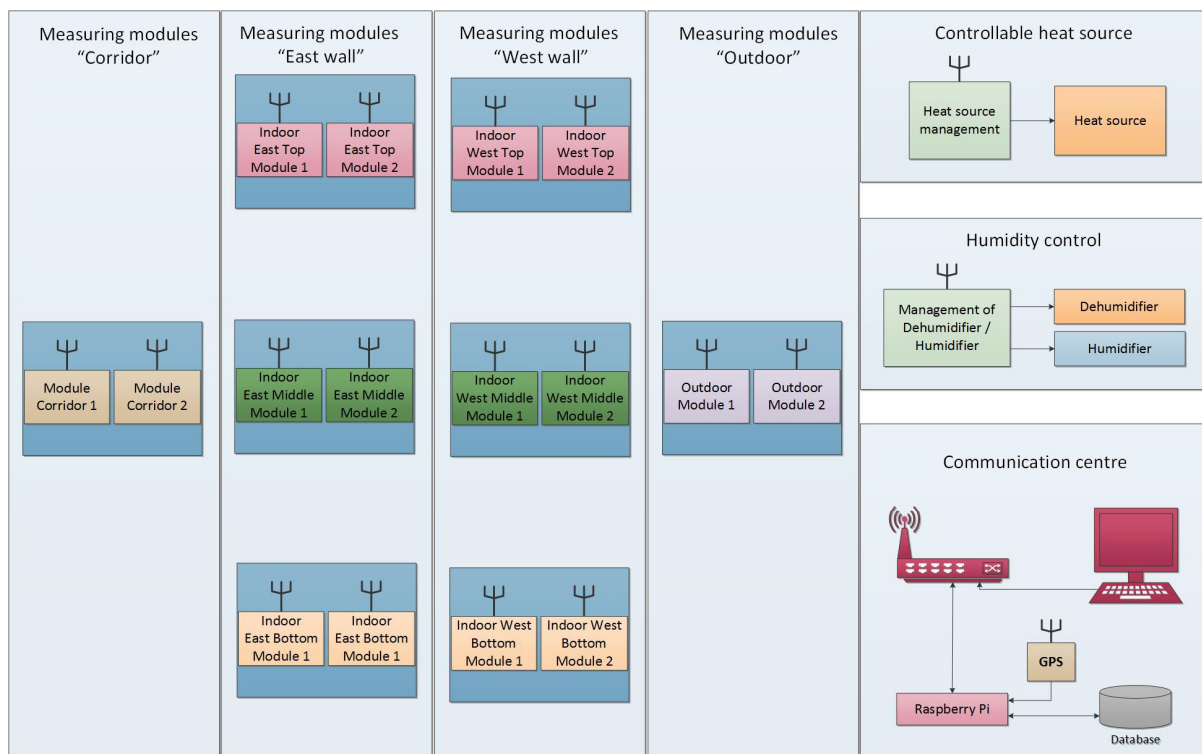


Figure 2. Structural scheme of the operation of a smart system enhancing comfort in dwellings.

The smart system for ensuring comfortable conditions in a dwelling is built on the basis of a single-board computer, Raspberry Pi [25,40,41]. Developed scripts scan each multifunctional sensor module at previously configured IP addresses, read the data, and save it to a file. There is also an option for asynchronous data retrieval from the measuring modules via events that are received when a message is published to the MQTT broker [23]. When recording data, two separate files in CSV format [42] are created for each day. The first file is created with the values of the measured parameters, taken every minute. The second file is created with the values of the measured parameters, taken every ten minutes.

The modules that measure atmospheric temperature and humidity have a BME280 barometric pressure sensor that also measures temperature and humidity, and these are implemented in the two outdoor modules. Modules measuring indoor temperature have a temperature sensor, MLX90614, which replaces the BME280 [43].

Connected to the single-board Raspberry Pi computer is an external GPS receiver, which provides UTC (universal coordinated time), avoiding the need for an external NTP (network time protocol) server [44] to synchronize the internal system clock of the Raspberry Pi. In this way, the system can be installed in a dwelling without needing to connect to the Internet. The external GPS module provides the time via a serial interface in a message with an NMEA 0183 format. Installed on the Raspberry Pi 3 is software for decoding the message, which receives the date and time, and then synchronizes the system clock of the single-board computer.

The NMEA 0183 standard describes the various types of messages transmitted by the GPS receiver to the device using it [45].

The single-board computer is connected to the router, allowing the developed scripts to access all multifunctional sensors.

Figure 3 depicts the algorithm of a software script that can be used to collect the microclimatic data from each pair of multifunctional modules. Each script runs on the operating system of the single-board computer every minute, based on specific events that have been developed in the OS. In step 1 of the algorithm, a request is sent to each of the pairs of measuring modules for the specific point. Once the data from the current measurement are received, it is processed in step 2 and is then saved to a file, as represented in Figure 3. After the data are saved to a file containing measurements taken every 1 min, step 3 checks the system time of the single-board computer for multiples of 10 min. If the time is a multiple of 10 min, in step 4, the same data are also saved to a file containing measurements taken every 10 min—step 5. At the end of the current day, a new file is created for the first measurements at 00:00 h of the following day.

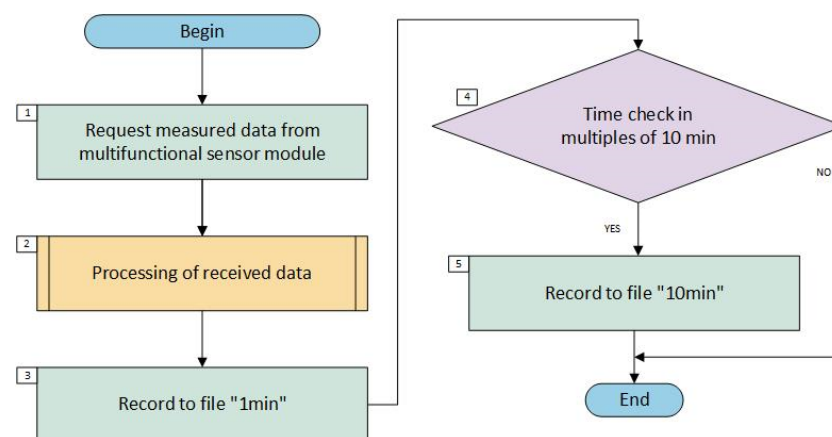


Figure 3. Flowchart of the algorithm for obtaining data from multifunction modules.

Integrating predictive models into IoT (Internet of Things) devices and systems represents the merging of two of the key areas of modern technology—data analytics and device connectivity. In the long term, this integration promises to transform the way our devices

work and interact with each other and with us, in the same way as would be useful in national monitoring systems [46].

In recent years, the capacity to collect and analyze information has grown exponentially. Predictive models based on artificial intelligence and machine learning are now capable of analyzing complex data sets and predicting behaviors or scenarios based on historical data. When these models are combined with IoT devices, the possibilities are endless. For example, air conditioning systems can anticipate changes in weather conditions and automatically adjust the temperature in your home or office. While long-term weather forecasts remain challenging, climate systems excel in short-term predictions and identifying trends. For instance, they can effectively anticipate sudden temperature fluctuations or shifts in humidity levels, enabling proactive adjustments in controlled environments [47].

Elsewhere, agricultural systems can analyze agricultural data and predict the best time to plant or water crops.

By introducing such predictive models into IoT devices, Internet-connected objects will not just respond to commands but will also anticipate user needs. This will make devices more adaptive, autonomous, and efficient.

Furthermore, the deployment of predictive models will accelerate innovation across multiple sectors, from medicine to industry and to urban planning. Cities could become smarter by optimizing traffic, managing their waste and resources more efficiently, and even predicting and preventing problems before they occur.

3. Time Series Analysis of Forecasting Relative Humidity in Dwellings

The study and prediction of relative humidity within residential environments are critical for ensuring comfortable living conditions and promoting the longevity and quality of people's lives. One of the most traditional and time-tested methods by which to analyze and predict such variables is through the classical approach of time series forecasting [48,49].

In essence, a time series is a sequence of observations taken sequentially in time. For relative humidity, this could be hourly readings of humidity percentages over several days, weeks, or even longer. The classical time series forecasting approach divides the time series into four constituent components: trend (T), seasonality (S), cyclic (C), and stochastic (I) components. Mathematically, the time series (Y) can be expressed as either an additive or multiplicative model [50]:

1. Additive model: $Y_t = T_t + S_t + C_t + I_t$
2. Multiplicative model: $Y_t = T_t \times S_t \times C_t \times I_t$

where:

- Y_t is the observed time series at time t ;
- T_t represents the trend component at time t ;
- S_t stands for the seasonality at time t ;
- C_t is the cyclic component at time t ;
- I_t denotes the stochastic or error component at time t .

The trend component captures the overall progression of the series, indicating whether the readings are generally increasing, decreasing, or stagnating over time. Seasonality captures repeating short-term fluctuations, which, in the context of humidity, might be the daily variations due to changes in temperature and other factors. The cyclic component is tied to business cycles and typically extends over longer periods. Finally, the irregular component captures random, unforeseeable fluctuations. To extract these components and forecast future values, classical techniques such as moving averages or exponential smoothing might be applied. For relative humidity, understanding and accurately predicting its levels using these foundational methods is crucial, not only for comfort but also for mold prevention, energy efficiency, and maintaining the overall health of a residence.

Experimental studies were carried out with the developed smart system in the period from 8 January 2018 to 10 January 2018. For this period of time, it is known that there were no visitors in the dwelling where the temperature and relative humidity were measured.

Figure 4 depicts the fluctuations in relative humidity over a 24-h period (*y*-axis of the graph) and the corresponding numerical values of time intervals (*x*-axis of the graph). The graph illustrates that the relative humidity inside the premises oscillated between approximately 42% and 48%.

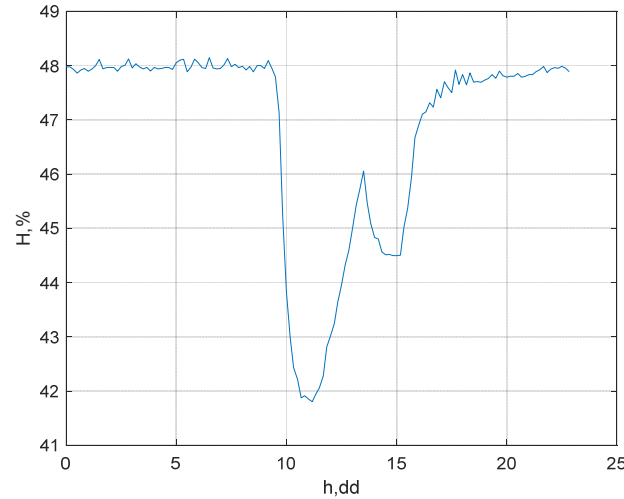


Figure 4. Changes in relative humidity for the defined period.

3.1. Trend Removal

Adhering to the approach used for temperature forecasting, the initial model employed here is a linear trend, as shown in Figure 5.

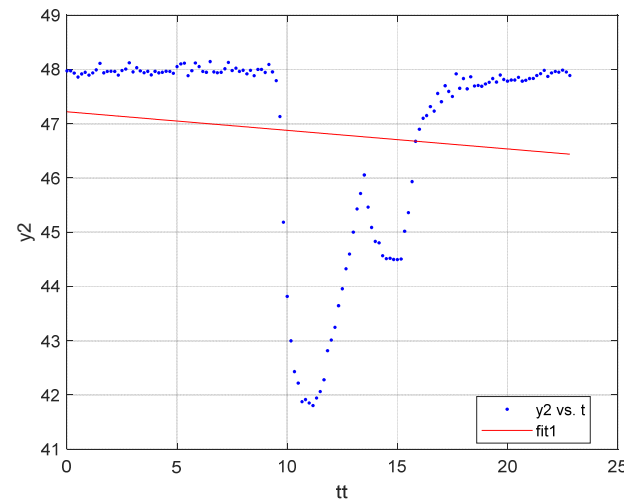


Figure 5. Real data and the linear trend.

The equation for this linear trend is provided as:

$$f(x) = p_1 \cdot x + p_2 \tag{1}$$

$$p_1 = -0.03425 \ (-0.0814, 0.0129)$$

$$p_2 = 47.22 \ (46.6, 47.84)$$

$$R^2: 0.2911$$

where *x* represents time, *f*(*x*) indicates temperature, and *p_i* are the sought-after coefficients in the model.

Figure 5 graphically showcases the actual variations in relative humidity, alongside the linear trend.

A notable observation from this representation is the negative trend. However, the low coefficient of determination suggests that this model can only account for nearly 30% of the error fluctuations. This necessitates the exploration of a more accurate model. After several iterations, a cubic trend model was chosen, the equation of which is given as:

$$f(x) = p_1 \cdot x^3 + p_2 \cdot x^2 + p_3 \cdot x + p_4 \tag{2}$$

$p_1 = 0.001599$ (0.0005243, 0.002673)
 $p_2 = -0.02717$ (-0.0645, 0.01017)
 $p_3 = -0.166$ (-0.5321, 0.2001)
 $p_4 = 48.67$ (47.71, 49.63)
 $R^2: 0.6961$

Figure 6 displays the actual measured humidity values, juxtaposed with the cubic trend.

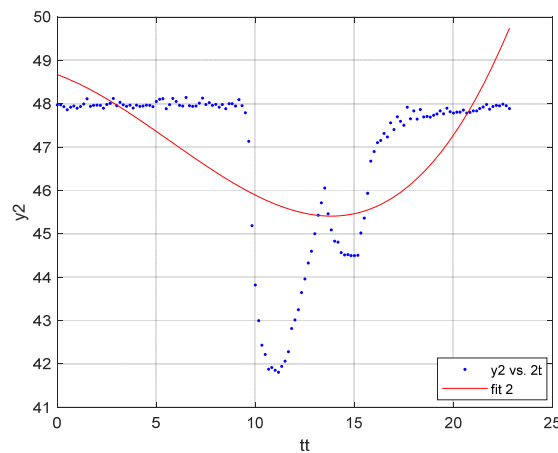


Figure 6. Real data and the cubic trend.

The derived results from the cubic trend model reveal that its coefficient of determination is significantly higher than that of the linear trend, meaning that it characterizes the data with greater precision. The confidence intervals are presented in brackets, assured at a probability of $\gamma = 0.95$.

After the trend removal (filtering) using both the linear and cubic models, the resulting plots are illustrated in Figures 7 and 8. From the plots, it is evident that when filtering the trend with the linear model, variations in relative humidity for the specific period range between -5% and $+1.5\%$. In contrast, filtering using the cubic model results in variations that are approximately from -4% to $+2\%$.

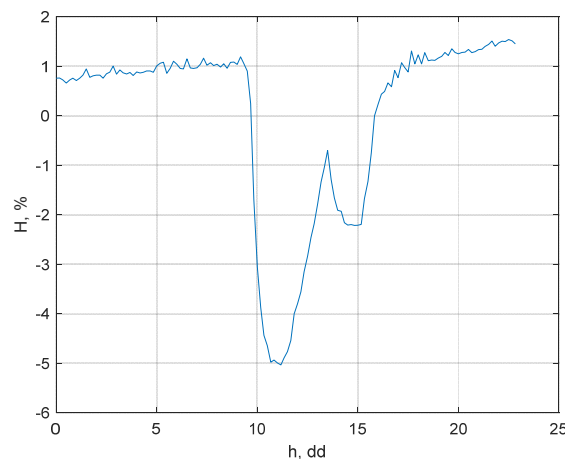


Figure 7. Detrending (filtration) with the linear model.

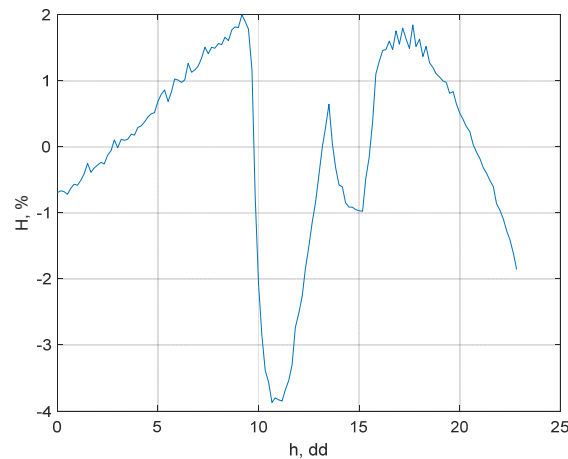


Figure 8. Detrending (filtration) with the cubic model.

3.2. Cyclicity

For the purposes of this study, there is an emphasis on seeking relatively simple models that can adequately approximate the data. After filtering the trend, experiments were conducted with four different periodicity models, with the results showcased in Figures 9–12. The chosen model is presented, followed by the coefficient values. Here, the cyclicity is described based on various models after trend filtering, using both linear and cubic approaches.

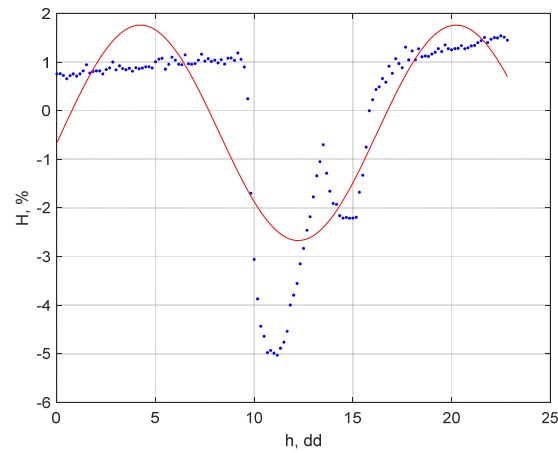


Figure 9. Fourier 1 model (blue dots—empirical data; red line—model output).

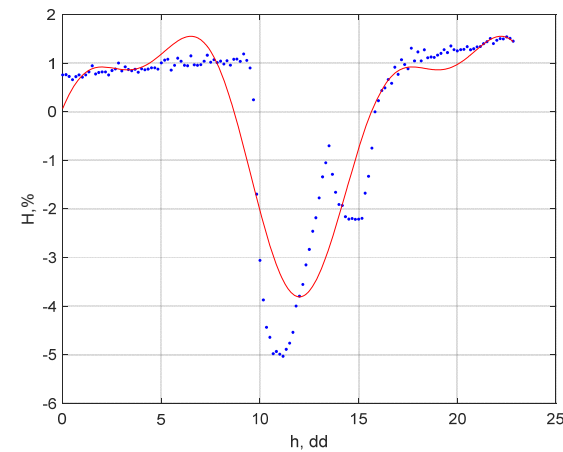


Figure 10. Fourier 2 model (blue dots—empirical data; red line—model output).

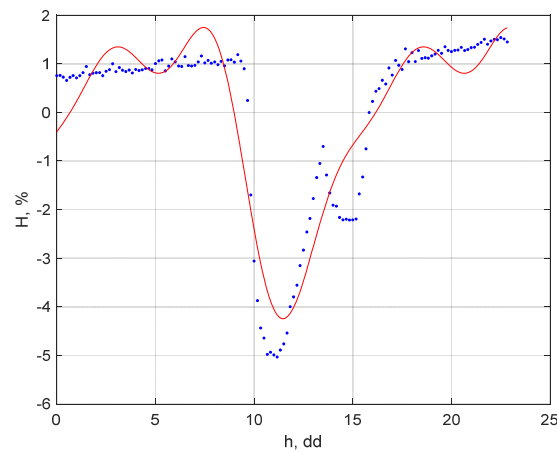


Figure 11. Fourier 3 model (blue dots—empirical data; red line—model output).

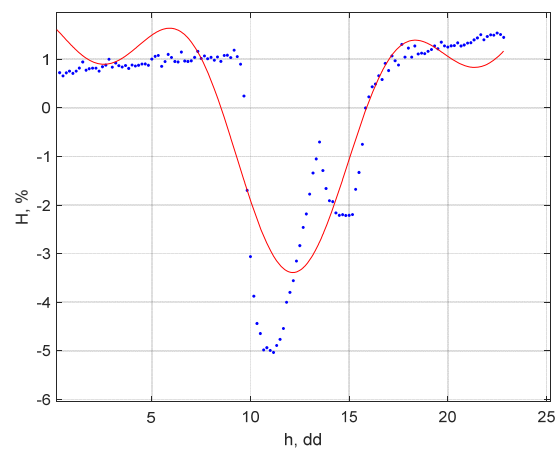


Figure 12. Sine model 2 (blue dots—empirical data; red line—model output).

Models describing the cyclicity of post-trend filtering with the linear model:
 General Fourier 1 model, as shown in Figure 9:

$$f(x) = a_0 + a_1 \cdot \cos(x.w) + b_1 \cdot \sin(x.w) \tag{3}$$

$$a_0 = -0.4569 \ (-0.6432, -0.2707)$$

$$a_1 = -0.2022 \ (-0.6958, 0.2914)$$

$$b_1 = 2.207 \ (1.949, 2.464)$$

$$w = 0.3928 \ (0.375, 0.4106)$$

General Fourier 2 model, as shown in Figure 10:

$$f(x) = a_0 + a_1 \cdot \cos(x.w) + b_1 \cdot \sin(x.w) + a_2 \cdot \cos(2.x.w) + b_2 \cdot \sin(2.x.w) \tag{4}$$

$$a_0 = -0.4643 \ (-0.6152, -0.3133)$$

$$a_1 = -0.4508 \ (-1.014, 0.1121)$$

$$b_1 = 2.346 \ (2.137, 2.554)$$

$$a_2 = 0.9776 \ (0.7776, 1.178)$$

$$b_2 = 0.04391 \ (-0.4696, 0.5574)$$

$$w = 0.3998 \ (0.3792, 0.4204)$$

General Fourier 3 model, as shown in Figure 11:

$$f(x) = a_0 + a_1 \cdot \cos(x.w) + b_1 \cdot \sin(x.w) + a_2 \cdot \cos(2.x.w) + b_2 \cdot \sin(2.x.w) + a_3 \cdot \cos(2.x.w) + b_3 \cdot \sin(2.x.w) \quad (5)$$

$$\begin{aligned} a_0 &= -0.4415 \quad (-0.5723, -0.3107) \\ a_1 &= -0.5854 \quad (-0.9797, -0.1912) \\ b_1 &= 2.325 \quad (2.142, 2.509) \\ a_2 &= 1.083 \quad (0.9013, 1.264) \\ b_2 &= 0.07387 \quad (-0.3489, 0.4966) \\ a_3 &= -0.4559 \quad (-0.7276, -0.1842) \\ b_3 &= -0.3771 \quad (-0.6341, -0.1201) \\ w &= 0.4056 \quad (0.3904, 0.4208) \end{aligned}$$

General sine model 2, as shown in Figure 12:

$$f(x) = a_1 \cdot \sin(b_1.x + c_1) + a_2 \cdot \sin(b_2.x + c_2) \quad (6)$$

$$\begin{aligned} a_1 &= 2.15 \quad (1.934, 2.367) \\ b_1 &= 0.3085 \quad (0.2819, 0.3351) \\ c_1 &= 0.9218 \quad (0.5813, 1.262) \\ a_2 &= 1.24 \quad (1.009, 1.471) \\ b_2 &= 0.6477 \quad (0.6099, 0.6856) \\ c_2 &= -3.119 \quad (-3.58, -2.659) \end{aligned}$$

Figure 9 models the cyclicity (after filtration with a linear trend) established with Equation (3), respectively. Figure 10 represents Equation (4), while Figure 11 depicts the cyclicity of form (5), and Figure 12 represents Equation (6).

The determination coefficients of the four cyclicity models, designated (3)–(6), after linear filtration are given in Figure 13.

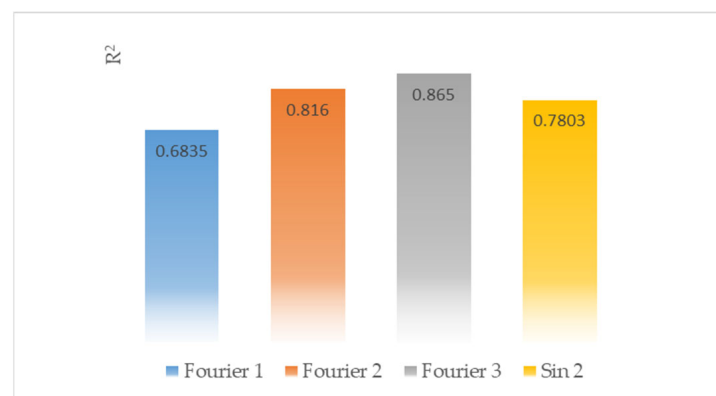


Figure 13. Determination coefficients for the different periodic models.

Upon analyzing the results, it is evident that the cyclicity is best described by the third model, Fourier 3. The coefficient of determination for this model is $R^2 = 0.865$, signifying that approximately 86.4% of the data variances are explained by this model.

Considering the equations for the linear trend and cyclicity, the composite model takes the following form:

$$\tilde{Y} = p_1x + p_0 + a_0 + a_1 \cdot \cos(x.w) + b_1 \cdot \sin(x.w) + a_2 \cdot \cos(2.x.w) + b_2 \cdot \sin(2.x.w) + a_3 \cdot \cos(2.x.w) + b_3 \cdot \sin(2.x.w) \tag{7}$$

When accounting for the linear trend and periodic cyclicity for time trend approximation, Equation (7) is derived. Figure 14 illustrates the plots for the approximation function based on Equation (7), juxtaposed with the actual data.

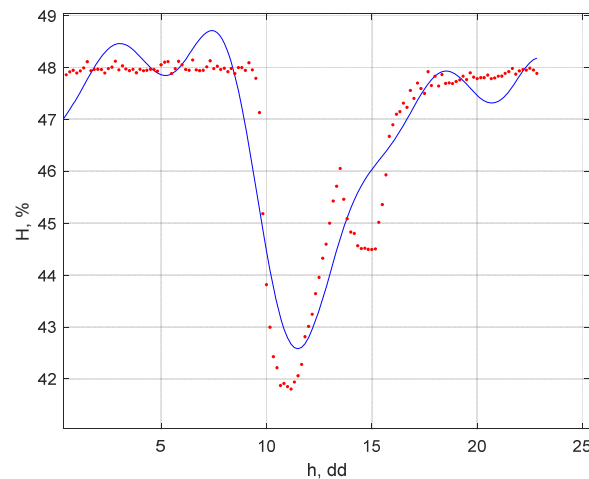


Figure 14. Approximation of function (7), with trend and cyclicity included (blue dots—empirical data; red line—model output).

One can infer that a substantial portion of the data is fairly approximated by the devised model. However, there are certain data points that diverge from the overall trend and model prediction, but they lie within the statistically reliable interval. Based on the conducted studies and analysis concerning seasonal variations and random fluctuations, model no. 4 is selected as the definitive model.

3.3. Model Validation

The logic behind the model validation mirrors the validation approach used for temperature forecasting. Figure 15 displays both the real and approximated values from the model’s validation for forecasting relative humidity in a dwelling. Figure 16a,b showcase the approximation errors in absolute and relative terms during the model’s validation.

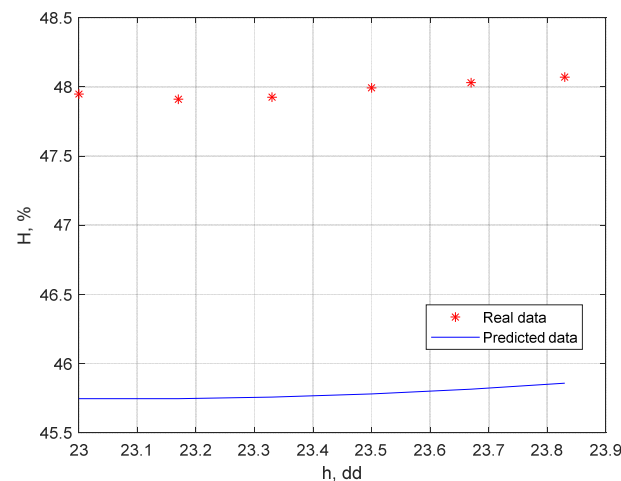


Figure 15. Real and approximated values in model validation.

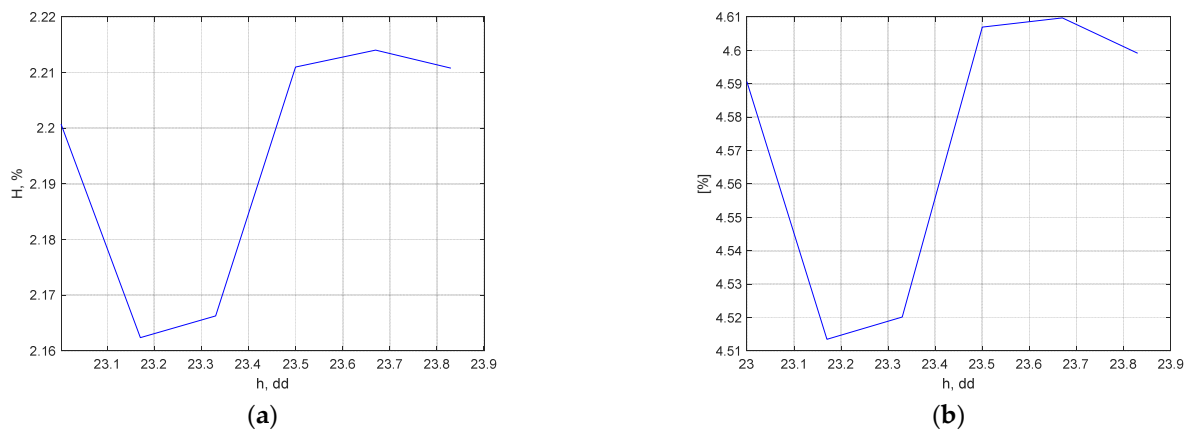


Figure 16. Absolute (a) and relative (b) model errors.

From the correlogram depicted in Figure 17, it is observable that the model performs aptly, with the dispersion around the straight line confirming this finding. The results suggest that post-validation, the relative errors in the model are below 5%, indicating the chosen model’s adequacy. The relative error between the actual and approximated data is roughly under 3%.

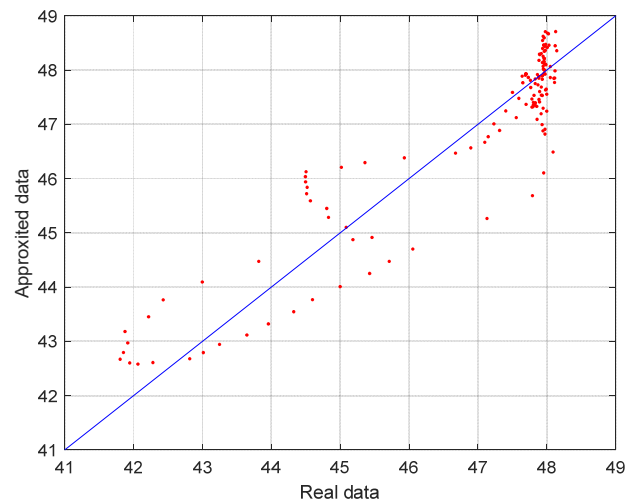


Figure 17. Correlogram of the real (red dots) and predicted (blue line) values.

Models describing the cyclicity after cubic model detrending:
 General Fourier 1 model, as shown in Figure 18:

$$f(x) = a_0 + a_1 \cdot \cos(x.w) + b_1 \cdot \sin(x.w) \tag{8}$$

$a_0 = -0.02288$ (−0.1953, 0.1496)
 $a_1 = -1.555$ (−1.803, −1.307)
 $b_1 = -0.2504$ (−0.7364, 0.2355)
 $w = 0.5382$ (0.5147, 0.5617)

General Fourier 2 model, as shown in Figure 19:

$$f(x) = a_0 + a_1 \cdot \cos(x.w) + b_1 \cdot \sin(x.w) + a_2 \cdot \cos(2.x.w) + b_2 \cdot \sin(2.x.w) \tag{9}$$

$$\begin{aligned}
 a_0 &= -0.06668 \quad (-0.2214, 0.08802) \\
 a_1 &= -1.62 \quad (-1.836, -1.405) \\
 b_1 &= -0.063 \quad (-0.4405, 0.3145) \\
 a_2 &= -0.3642 \quad (-0.655, -0.0733) \\
 b_2 &= 0.5261 \quad (0.2885, 0.7638) \\
 w &= 0.5296 \quad (0.514, 0.5451)
 \end{aligned}$$

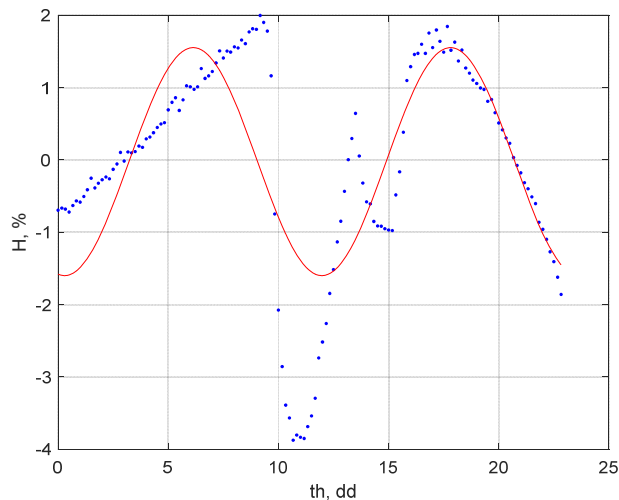


Figure 18. Fourier 1 model (blue dots—empirical data; red line—model output).

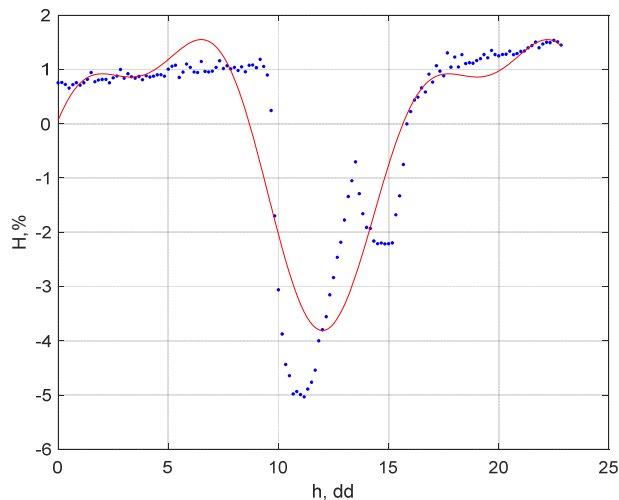


Figure 19. Fourier 2 model (blue dots—empirical data; red line—model output).

General Fourier 3 model, as shown in Figure 20:

$$\begin{aligned}
 f(x) = & a_0 + a_1 \cdot \cos(x.w) + b_1 \cdot \sin(x.w) \\
 & + a_2 \cdot \cos(2.x.w) \\
 & + b_2 \cdot \sin(2.x.w) \\
 & + a_3 \cdot \cos(2.x.w) \\
 & + b_3 \cdot \sin(2.x.w)
 \end{aligned} \tag{10}$$

$$\begin{aligned}
 a_0 &= -0.1678 \quad (-0.2857, -0.04981) \\
 a_1 &= -1.72 \quad (-1.881, -1.558) \\
 b_1 &= 0.2894 \quad (0.05029, 0.5285) \\
 a_2 &= -0.2711 \quad (-0.4703, -0.07186) \\
 b_2 &= 0.6734 \quad (0.4996, 0.8472)
 \end{aligned}$$

$a_3 = 0.1681 (-0.08261, 0.4187)$
 $b_3 = 0.7384 (0.5675, 0.9093)$
 $w = 0.5154 (0.5078, 0.523)$
 R-square: 0.864

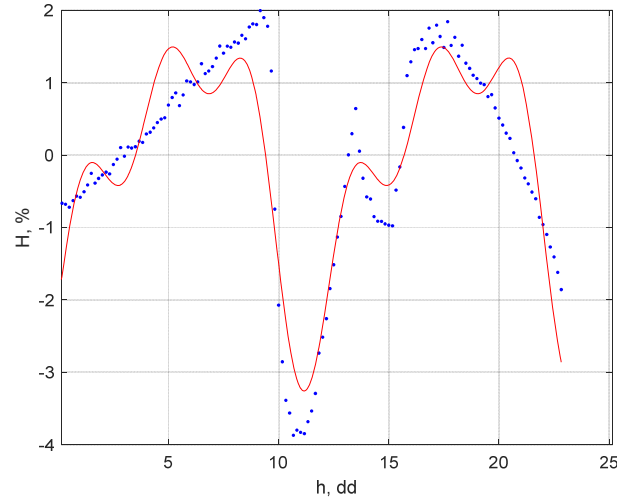


Figure 20. Fourier 3 model (blue dots—empirical data; red line—model output).

General Sine 2 model, as shown in Figure 21:

$$f(x) = a_1 \cdot \sin(b_1 \cdot x + c_1) + a_2 \cdot \sin(b_2 \cdot x + c_2) \tag{11}$$

$a_1 = 1.627 (1.429, 1.824)$
 $b_1 = 0.5404 (0.5222, 0.5586)$
 $c_1 = -1.741 (-1.988, -1.494)$
 $a_2 = 0.6887 (0.4936, 0.8838)$
 $b_2 = 1.548 (1.506, 1.59)$
 $c_2 = 0.2426 (-0.3189, 0.8042)$

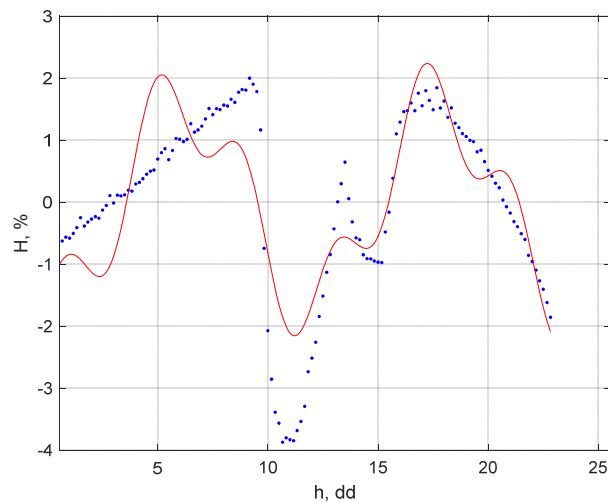


Figure 21. Sine 2 model (blue dots—empirical data; red line—model output).

Figure 18 models the cyclicity (after filtration with the cubic trend) with Equation (8), respectively. Figure 19 represents Equation (9), Figure 20 depicts the cyclicity of Equation (10), and Figure 21 represents Equation (11).

Upon analyzing the results, it becomes evident that among the proposed four models, the cyclicity is best captured by model no. 3, denoted as Fourier 3 in Equation (10).

Figure 22 presents the coefficients of determination of the cyclicity models (8)–(11) after cubic filtration.

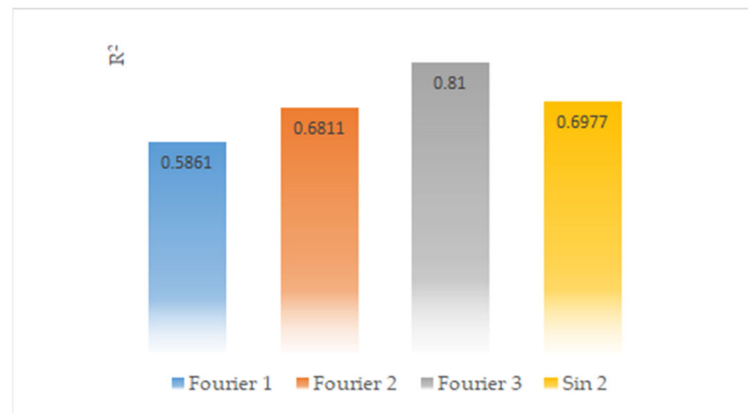


Figure 22. Determination coefficients of the different periodic models.

The graph indicates that out of the four proposed models, model no. 3 provides a robust representation of cyclicity. The coefficient of determination for this model is approximately $R^2 = 0.81$, signifying that around 81% of the variances in the data are accounted for by this model.

Considering the cubic trend and cyclicity equations, the comprehensive model is formulated as:

$$\begin{aligned} \tilde{Y} = & p_3x^3 + p_2x^2 + p_1x + p_0 + a_0 + \\ & a_1 \cdot \cos(x.w) + b_1 \cdot \sin(x.w) + a_2 \cdot \cos(2.x.w) + \\ & b_2 \cdot \sin(2.x.w) + a_3 \cdot \cos(2.x.w) + \\ & b_3 \cdot \sin(2.x.w) \end{aligned} \tag{12}$$

Figure 23 showcases the approximating function incorporating both the trend and the cyclicity.

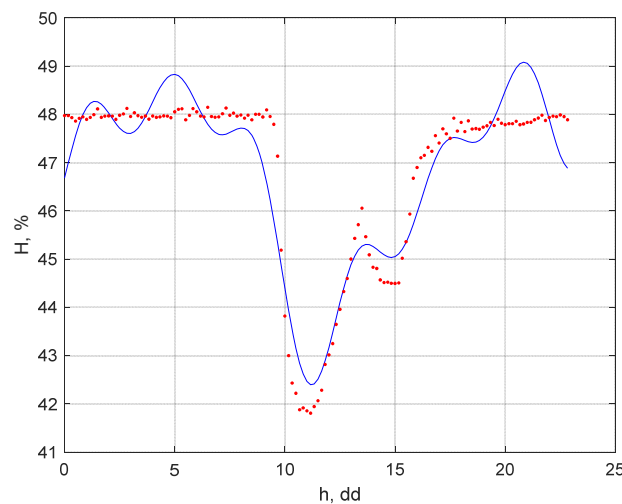


Figure 23. Approximation of function (12), with included trend and cyclicity (blue dots—empirical data; red line—model output).

When the cubic trend and periodic cyclicity are taken into account for time trend approximation, we arrive at Equation (12). Its graphical representation is depicted in Figure 23, portraying the approximation function against the actual measured values.

The analysis reveals that a substantial portion of the data is approximated well by the established model. However, there are specific data points that deviate from the general

trend and the model's forecast, yet they lie within the statistically significant interval. Based on extensive research and analysis concerning seasonal variations and anomalies, model no. 3 is chosen as the final model.

3.4. Model Validation

Figure 24 illustrates the actual and approximated values derived from the model's validation. From Figure 25, it is discernible that the model performs consistently, with the scattering around the line affirming this behavior.

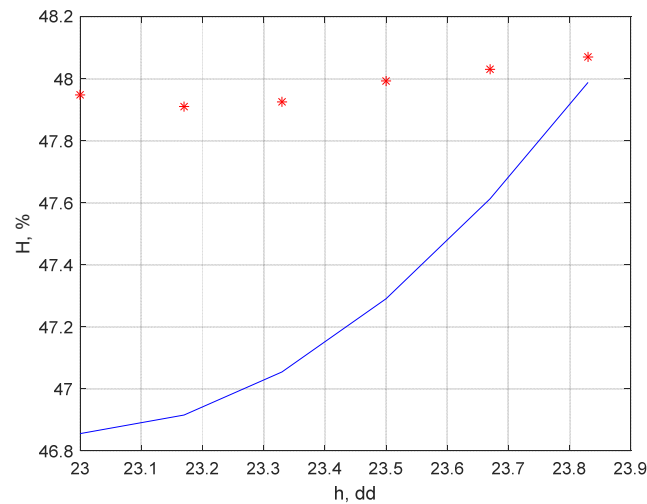


Figure 24. Real (red asterisks) and approximated (blue line) values in the model validation.

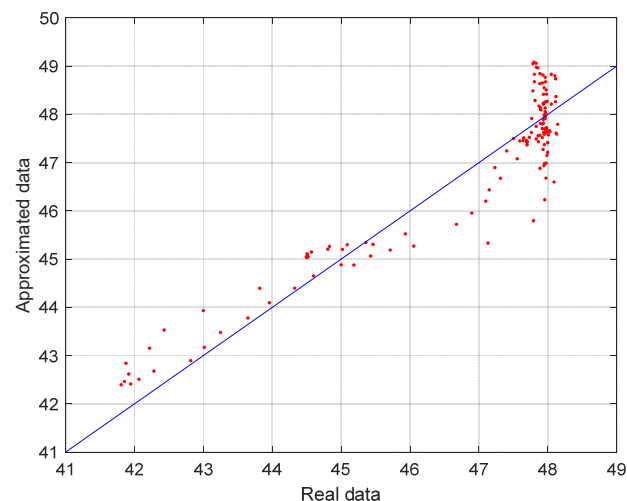


Figure 25. Correlogram of the real (red dots) and forecasted (blue line) values.

Figure 26a,b depict the errors in the approximated data in both absolute and relative terms during the model's validation.

The relative error between the actual and approximated data is approximately $\pm 0.1\%$. The obtained results confirm that post-validation, the relative errors in the model are less than 2.5%, thereby substantiating the model's adequacy.

The research outcomes suggest that by forecasting humidity over time, one can optimize the activation timing of a dehumidifier or air humidifier. This ensures the achievement of the desired comfort conditions, with minimal energy consumption. Based on the traditional forecasting of relative humidity, sections of Figure 27a,b have been constructed, founded on the coordinates of the relative humidity measurement sensors, comprising six in total.

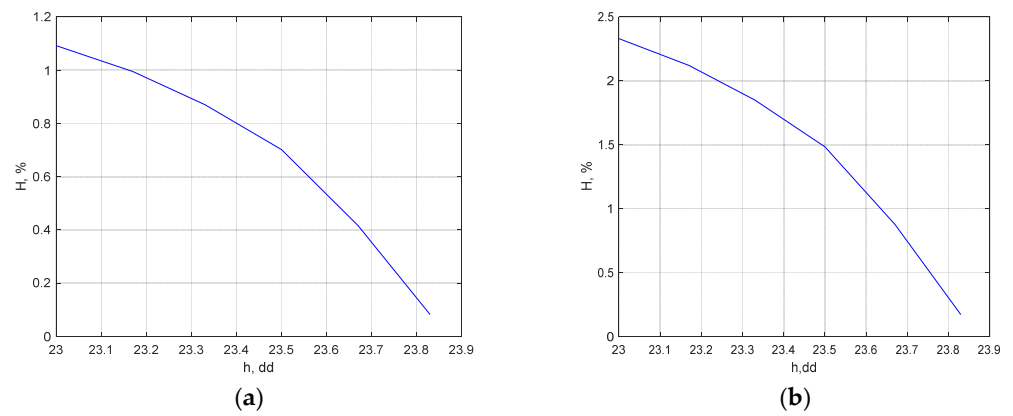


Figure 26. Absolute (a) and relative (b) model errors.

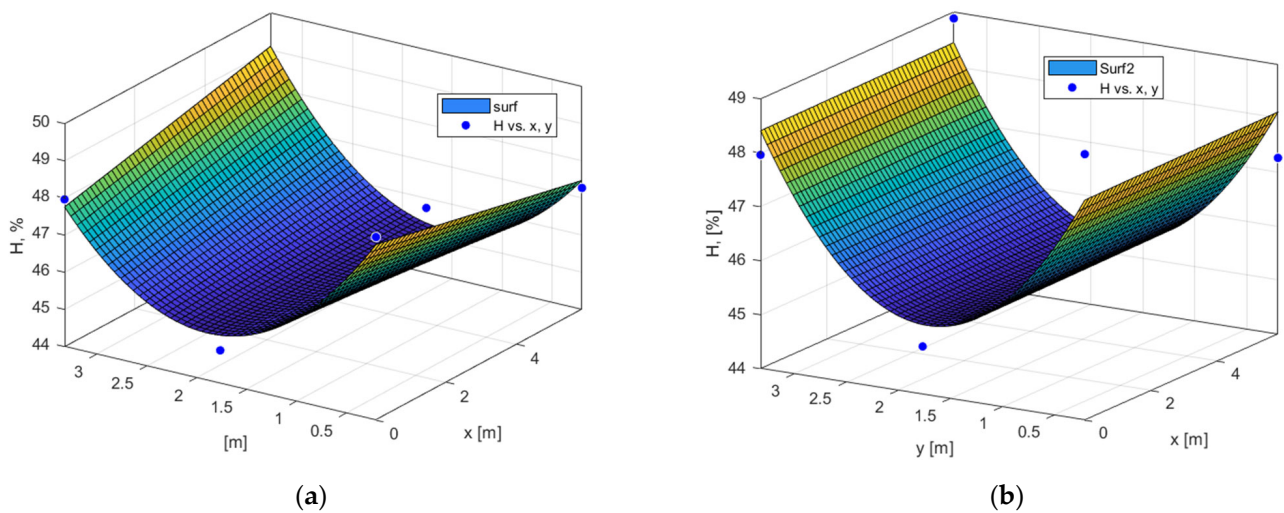


Figure 27. Cross-section of the dwelling with the forecasted relative humidity. (a)—model Poly12; (b)—general model.

For building the module, the next models to be used are:

Incomplete quadratic polynomial in two variables (Model Poly12), shown in Figure 27a:

$$f(x, y) = p_{00} + p_{10} \cdot x + p_{01} \cdot y + p_{11} \cdot x \cdot y + p_{02} \cdot y^2 \tag{13}$$

$$\begin{aligned} p_{00} &= 49.6 \\ p_{10} &= -0.2449 \\ p_{01} &= -4.578 \\ p_{11} &= 0.1423 \\ p_{02} &= 1.213 \\ R^2 &= 0.9648 \end{aligned}$$

Incomplete quadratic polynomial in two variables (general model), shown in Figure 27b:

$$f(x, y) = p_{00} + p_{10} \cdot x + p_{01} \cdot y + p_{02} \cdot y^2 \tag{14}$$

$$\begin{aligned} p_{00} &= 48.86 \\ p_{10} &= 0.005527 \\ p_{01} &= -4.162 \\ p_{02} &= 1.213 \\ R^2 &= 0.8435 \end{aligned}$$

4. Conclusions

A smart system for enhancing comfort in dwellings has been developed, in which a predictive time series model has been implemented in the operating algorithm. The studies conducted herein show that predictive time series models require fewer computational resources and less data volume compared to deep learning-based methods, which would help to optimize, control, and improve the environmental factors in a room and in real time.

Indoor relative humidity is an object of prediction, as it is one of the main factors through which various aspects of the air environment, including the concentration of fine particulate matter, can be controlled [51,52], thereby aiming to achieve a comfortable and healthy environment for building occupants [53].

This research presents a fundamental approach to enhancing residential comfort through the implementation of a predictive model in a smart system. The paper's major contribution lies in the development and validation of model no. 3, based on the Fourier 3 equation, which excels in accurately forecasting the relative humidity within residential spaces. This model demonstrates remarkable efficiency, capturing approximately 81% of data variances, with a minimal error margin of $\pm 0.1\%$. Furthermore, the study bridges the gap between advanced predictive analytics and practical application, showcasing how accurate humidity forecasts can lead to the optimized operation of household devices like dehumidifiers and air humidifiers. This not only elevates indoor comfort levels but also promotes energy efficiency, offering a sustainable solution for modern living environments. The paper's findings represent a significant step forward in the realm of home automation and sustainable residential design.

Furthermore, the implications of our findings extend beyond mere comfort. In an era where sustainability is paramount, the ability to accurately predict and thereby efficiently manage indoor conditions can lead to significant energy savings. Optimized operations of devices like dehumidifiers and air humidifiers, when driven by our predictive model, can ensure a comfortable indoor atmosphere while conserving energy. This harmonious blend of comfort and sustainability, as underscored by our research, paves the way for future residential setups where well-being coexists seamlessly with ecological responsibility.

This work could be further developed in a number of ways. For instance, the forecasting procedure could be improved by means of more advanced and sophisticated approaches, such as (S)ARIMA-type methods, neural networks (including CNN and LSTM), modified ODEs, etc. What is more, the humidity and temperature could be considered together as exogenous inputs. It would also be useful to study the impact of humidity dynamics on the residing people.

Author Contributions: Conceptualization, S.Z. and I.G.; methodology, S.Z. and I.G.; software, I.G. and S.G.; validation, S.Z. and I.S.; formal analysis, I.G.; investigation, S.Z. and I.G.; resources, I.S.; data curation, I.G. and S.G.; writing—original draft preparation, S.Z., I.G. and S.G.; writing—review and editing, S.Z., I.G., S.G., I.S. and A.B.; visualization, I.G.; supervision, S.Z., I.G. and S.G.; project administration, S.G.; funding acquisition, I.G. and S.G. All authors have read and agreed to the published version of the manuscript.

Funding: This study is supported by the BG05M2OP001-1.001-0004 UNITE project, funded by the Operational Program "Science and Education for Smart Growth", co-funded by the European Union through the European Structural and Investment Funds.

Data Availability Statement: The data used in this study are available from the authors upon request.

Acknowledgments: The authors would like to thank the anonymous reviewers for their constructive comments, which have significantly improved the quality of the paper.

Conflicts of Interest: The authors declare no conflict of interest. The funders had no role in the design of the study; in the collection, analyses, or interpretation of data; in the writing of the manuscript; or in the decision to publish the results.

References

1. Wolkoff, P. Indoor air humidity, air quality, and health—An overview. *Int. J. Hyg Environ. Health* **2018**, *221*, 376–390. [CrossRef] [PubMed]
2. Deng, Y.; Feng, Z.; Fang, J.; Cao, S.J. Impact of ventilation rates on indoor thermal comfort and energy efficiency of ground-source heat pump system. *Sustain. Cities Soc.* **2018**, *37*, 154–163. [CrossRef]
3. Bornehag, C.G.; Blomquist, G.; Gyntelberg, F.; Jarvholm, B.; Malmberg, P.; Nordvall, L.; Sundell, J. Dampness in buildings and health. Nordic interdisciplinary review of the scientific evidence on associations between exposure to “dampness” in buildings and health effects (NORDDAMP). *Indoor Air* **2001**, *11*, 72–86. [CrossRef] [PubMed]
4. Aizlewood, C.E.; Coward, S.K.D.; Hamilton, L.; Raw, G.J.; Wilde, D.J. The impact of humidity on health and comfort in an office building. In Proceedings of the 9th International Conference on IAQ & Climate, Santa Cruz, CA, USA, 30 June–5 July 2002; Volume 4.
5. Candas, V. Confort thermique. *Technique de L'ingénieur, Traité de Génie Energétique* 2000. Available online: <https://www.techniques-ingenieur.fr/base-documentaire/archives-th12/archives-ressources-energetiques-et-stockage-tiabebe/archive-1/confort-thermique-be9085/qu-est-ce-que-le-confort-thermique-be9085niv10001.html> (accessed on 22 October 2023).
6. Oh, S.; Song, S. Detailed Analysis of Thermal Comfort and Indoor Air Quality Using Real-Time Multiple Environmental Monitoring Data for a Childcare Center. *Energies* **2021**, *14*, 643. [CrossRef]
7. Toftum, J.; Fanger, P.O. Air humidity requirements for human comfort. *ASHRAE Trans.* **1999**, *105*, 641.
8. Todorov, V.; Dimov, I. Unveiling the Power of Stochastic Methods: Advancements in Air Pollution Sensitivity Analysis of the Digital Twin. *Atmosphere* **2023**, *14*, 1078. [CrossRef]
9. Hashiguchi, N.; Hirakawa, M.; Tochihara, Y.; Kaji, Y.; Karaki, C. Effects of humidifiers on thermal conditions and subjective responses of patients and staff in a hospital during winter. *Appl. Ergon.* **2007**, *39*, 158–165. [CrossRef]
10. Baughman, A.; Arens, E.A. Indoor humidity and human health: Part 1—Literature review of health effects of humidity-influenced indoor pollutants. *Indoor Environ. Qual. (IEQ)* **1996**, *102*, 193–211.
11. Sunwoo, Y.; Chou, C.; Takeshita, J.; Murakami, M.; Tochihara, Y. Physiological and subjective responses to low relative humidity in young and elderly men. *J. Physiol. Anthropol.* **2006**, *25*, 229–238. [CrossRef]
12. Frontczak, M.; Wargocki, P. Literature survey on how different factors influence human comfort in indoor environments. *Build. Environ.* **2011**, *46*, 922e37. [CrossRef]
13. Zalejska-Jonsson, A.; Wilhelmsson, M. Impact of perceived indoor environment quality on overall satisfaction in Swedish dwellings. *Build. Environ.* **2013**, *63*, 134e44. [CrossRef]
14. El-Leathey, L.-A.; Anghelita, P.; Constantin, A.-I.; Circumaru, G.; Chihaia, R.-A. System for Indoor Comfort and Health Monitoring Tested in Office Building Environment. *Appl. Sci.* **2023**, *13*, 11360. [CrossRef]
15. Zaharieva, S.; Stoev, I. *Ensuring Comfortable Conditions in a Residential Premises Based on Predictable Models and Internet of Things*; Ruse University Press: Ruse, Bulgaria, 2022; ISBN 978-954-712-885-9.
16. Liu, Y.; Zhou, G. Key technologies and applications of internet of things. In Proceedings of the 2012 Fifth International Conference on Intelligent Computation Technology and Automation, Zhangjiajie, China, 12–14 January 2012; pp. 197–200.
17. He, X. A Survey on Time Series Forecasting. In *3D Imaging—Multidimensional Signal Processing and Deep Learning. Smart Innovation, Systems and Technologies*; Patnaik, S., Kountchev, R., Tai, Y., Kountcheva, R., Eds.; Springer: Singapore, 2023; Volume 348. [CrossRef]
18. Almeida, A.; Brás, S.; Sargento, S. Time series big data: A survey on data stream frameworks, analysis and algorithms. *J. Big Data* **2023**, *10*, 83. [CrossRef] [PubMed]
19. Hahn, Y.; Langer, T.; Meyes, R.; Meisen, T. Time Series Dataset Survey for Forecasting with Deep Learning. *Forecasting* **2023**, *5*, 315–335. [CrossRef]
20. Manowska, A.; Wycisk, A.; Nowrot, A.; Pielot, J. The Use of the MQTT Protocol in Measurement, Monitoring and Control Systems as Part of the Implementation of Energy Management Systems. *Electronics* **2023**, *12*, 17. [CrossRef]
21. Kodali, R.; Mahesh, K. A low cost implementation of MQTT using ESP8266. In Proceedings of the 2016 2nd International Conference on Contemporary Computing and Informatics (IC3I), Noida, India, 14–17 December 2016; pp. 404–408. [CrossRef]
22. Soni, D.; Makwana, A. A survey on MQTT: A protocol of internet of things (IoT). In Proceedings of the International Conference on Telecommunication, Power Analysis and Computing Techniques (Ictpact—2017), Chennai, India, 6–8 April 2017; Bharath Institute of Higher Education and Research: Chennai, India, 2017; pp. 173–177.
23. Stoev, I.; Zaharieva, S.; Borodzhieva, A.; Staevska, G. An Approach for Securing MQTT Protocol in ESP8266 WiFi Module. In Proceedings of the 2020 XI National Conference with International Participation (ELECTRONICA), Sofia, Bulgaria, 23–24 July 2020; pp. 1–4. [CrossRef]
24. Yan, H.; Hejun, Y.; Yuan, G.; Han, Z.; Yuan, X. Development of the high real-time GPS time transfer receiver. In Proceedings of the 29th Conference on Precision Electromagnetic Measurements (CPEM 2014), Rio de Janeiro, Brazil, 24–29 August 2014; pp. 150–151. [CrossRef]
25. Stoev, I.; Zaharieva, S.; Mutkov, V.; Petrova, T. An Approach for Modelling Energy Flows in Residential Premises. In Proceedings of the 2021 12th National Conference with International Participation (ELECTRONICA), Sofia, Bulgaria, 27–28 May 2021; pp. 1–4. [CrossRef]
26. Powers, E.; Hahn, J. GPS and Galileo UTC time distribution. In Proceedings of the 18th European Frequency and Time Forum (EFTF 2004), Guildford, UK, 5–7 April 2004. [CrossRef]

27. Rajput, A.K.; Tewani, R.; Dubey, A. The helping protocol “DHCP”. In Proceedings of the 2016 3rd International Conference on Computing for Sustainable Global Development (INDIACom), New Delhi, India, 16–18 March 2016; pp. 634–637.
28. Stoev, I.I.; Zaharieva, S.L.; Borodzhieva, A.N. An Approach for Assessment of the Synchronization Between Digital Temperature Sensors. In Proceedings of the 2019 27th Telecommunications Forum (TELFOR), Belgrade, Serbia, 26–27 November 2019; pp. 1–4. [[CrossRef](#)]
29. Stoev, I.I.; Zaharieva, S.L.; Mutkov, V.A. Evaluation of Gross Errors in Measured Temperature with an Electronic System for Management of Residential Energy Systems. In Proceedings of the 2019 27th Telecommunications Forum (TELFOR), Belgrade, Serbia, 26–27 November 2019; pp. 1–4. [[CrossRef](#)]
30. Zaharieva, S.; Stoev, I.; Borodzhieva, A.; Petrova, T. Assessment of Gross Errors and Uniformity of Readings of Sensors for Relative Humidity Measurement in Indoor Premises. In Proceedings of the 2023 22nd International Symposium Infoteh-Jahorina (Infoteh), Jahorina, Istočno Sarajevo, Bosnia and Herzegovina, 15–17 March 2023; pp. 1–5. [[CrossRef](#)]
31. Sindhuja, P.; Balamurugan, S. Smart Power Monitoring and Control System through Internet of Things using Cloud Data Storage. *Indian J. Sci. Technol.* **2023**, *8*, 1–8. [[CrossRef](#)]
32. Ekwevugbe, T.; Brown, N.; Pakka, V.; Fan, D. Real-time Building Occupancy Sensing Neural-Network Based Sensor Network. In Proceedings of the 2013 7th IEEE International Conference on Digital Ecosystems and Technologies (DEST), Menlo Park, CA, USA, 24–26 July 2013; pp. 114–119. [[CrossRef](#)]
33. Erickson, V.; Lin, Y.; Kamthe, A.; Brahme, R.; Surana, A.; Cerpa, A.; Sohn, M.; Narayanan, S. Energy efficient building environment control strategies using real-time occupancy measurements. In Proceedings of the First ACM Workshop on Embedded Sensing Systems for Energy-Efficiency in Buildings, New York, NY, United States, 3 November 2009.
34. IRC3000. *IRC3000 Series People Counting Camera*; InfraRed Integrated Systems Limited: Northampton, UK, 2010.
35. Lu, J.; Sookoor, T.; Srinivasan, V.; Gao, G.; Holben, B.; Stankovic, J.; Field, E.; Whitehouse, K. The Smart Thermostat Using Occupancy Sensors to Save Energy in Homes. In Proceedings of the 8th ACM Conference on Embedded Networked Sensor Systems, Zürich, Switzerland, 3–5 November 2010; pp. 211–224. [[CrossRef](#)]
36. Nguyen, T.; Aiello, M. Beyond Indoor Presence Monitoring with Simple Sensors. In Proceedings of the International Conference on Pervasive and Embedded Computing and Communication Systems, Rome, Italy, 24–26 February 2012.
37. Garg, V.; Bansal, N. Smart Occupancy sensors to reduce energy consumption. *Energy Build.* **2000**, *32*, 81–87. [[CrossRef](#)]
38. Hitiyise, E.; Ntagwirumugara, E.; Habarurema, W.; Ingabire, W.; Gasore, G. Building occupancy detection through sensor belief networks. *Int. J. Appl. Eng. Res.* **2016**, *11*, 10414–10419.
39. Kashif, A.; Le, X.; Dugdale, J.; Ploix, S. Agent Based Framework to Simulate Inhabitants’Behaviour in Domestic Settings for Energy Management. In Proceedings of the 3rd International Conference on Agents and Artificial Intelligence, Rome, Italy, 28–30 January 2011; Volume 2.
40. Kanaga Sura Raja, S.; Viswanathan, C.; Sivakumar, D.; Vivekanandan, M. Secured Smart Home Energy Monitoring System (Sshems) Using Raspberry Pi. *J. Theor. Appl. Inf. Technol.* **2014**, *66*, 305–314.
41. Rao, P.; Uma, S. Raspberry Pi Home Automation with Wireless Sensors Using Smart Phone. *Int. J. Comput. Sci. Mob. Comput.* **2015**, *5*, 797–803.
42. Alfathdyanto, K.; Febrianti, M.S.; Prihatmanto, A.S.; Machbub, C. Creating Database for Traditional Dance Categorization using CSV File Format. In Proceedings of the 2018 IEEE 8th International Conference on System Engineering and Technology (ICSET), Bandung, Indonesia, 15–16 October 2018; pp. 167–171. [[CrossRef](#)]
43. Stoev, I. *ESP8266 Based Multifunctional Module for Measuring Microclimatic Data*; University of Ruse “Angel Kanchev”: Ruse, Bulgaria, 2019; ISBN 1311-3321.
44. Nakashima, T.; Oshima, S.; Nakashima, A. Implementation of the performance evaluation system for the NTP server. In Proceedings of the 2003 IEEE Pacific Rim Conference on Communications Computers and Signal Processing (PACRIM 2003) (Cat. No.03CH37490), Victoria, BC, Canada, 28–30 August 2003; Volume 2, pp. 828–831. [[CrossRef](#)]
45. Shoab, M.; Jain, K.; Anulhaq, M.; Shashi, M. Development and implementation of NMEA interpreter for real time GPS data logging. In Proceedings of the 2013 3rd IEEE International Advance Computing Conference (IACC), Ghaziabad, India, 22–23 February 2013; pp. 143–146. [[CrossRef](#)]
46. Burdzhiev, S.D.; Georgiev, G. National system for complex monitoring. In Proceedings of the Collection of Materials from the Third National Conference with International Participation “Metallurgy, Hydro- and Aerodynamics, National Security, Sofia, Bulgaria, 2013; pp. 458–8308, ISBN 1313-8308.
47. Rožanec, J.; Trajkova, E.; Kenda, K.; Fortuna, B.; Mladenčić, D. Explaining Bad Forecasts in Global Time Series Models. *Appl. Sci.* **2021**, *11*, 9243. [[CrossRef](#)]
48. Gocheva, S.G. Lectures on Econometrics, European Virtual Laboratory of Mathematics. Available online: <https://www.fmi-plovdiv.org/evlm/DBbg/bmatmenu/> (accessed on 22 November 2023).
49. Adhikari, R.; Agrawal, R.K. *An Introductory Study on Time Series Modeling and Forecasting*; Cornell University: Ithaca, NY, USA, 2013; p. 68.
50. Hyndman, R.J.; Athanasopoulos, G. *Forecasting: Principles & Practice*, 3rd ed.; Otexts: Melbourne, Australia, 2021.

51. Communication from the Commission to the European Parliament, the Council, the European Economic and Social Committee and the Committee of the Regions A Europe that Protects: Clean Air for All; COM(2018) 330 final; European Commission: Brussels, Belgium. 2018. Available online: <https://eur-lex.europa.eu/legal-content/EN/TXT/PDF/?uri=CELEX:52018DC0330> (accessed on 15 November 2023).
52. Yankov, E. Hristov and Tzvetelin Gueorguiev. In A critical overview of the normative, regulatory and international standard requirements for healthy and safe public facilities. In Proceedings of the 2022 8th International Conference on Energy Efficiency and Agricultural Engineering (EE&AE), Ruse, Bulgaria, 30 June–2 July 2022; pp. 1–4.
53. Ministry of Labour and Social Policy; Ministry of Health. REGULATION No. RD-07-3 of 18 July 2014 on the Minimum Requirements for the Microclimate at Workplaces. *State Gazette* **2014**, 63, 52.

Disclaimer/Publisher's Note: The statements, opinions and data contained in all publications are solely those of the individual author(s) and contributor(s) and not of MDPI and/or the editor(s). MDPI and/or the editor(s) disclaim responsibility for any injury to people or property resulting from any ideas, methods, instructions or products referred to in the content.